Electronic Structures and Optical Absorption Properties of Ni-doped Anatase TiO2 for Photocatalysis from First-Principles Calculation

M. Liu, Z. Zhou, M. Li, L. Guo

This document appeared in

Detlef Stolten, Thomas Grube (Eds.):
18th World Hydrogen Energy Conference 2010 - WHEC 2010
Parallel Sessions Book 3: Hydrogen Production Technologies - Part 2
Proceedings of the WHEC, May 16.-21. 2010, Essen
Schriften des Forschungszentrums Jülich / Energy & Environment, Vol. 78-3
Institute of Energy Research - Fuel Cells (IEF-3)
Forschungszentrum Jülich GmbH, Zentralbibliothek, Verlag, 2010
ISBN: 978-3-89336-653-8

Electronic Structures and Optical Absorption Properties of Ni-doped Anatase TiO_2 for Photocatalysis from First-Principles Calculation

Maochang Liu, Zhaohui Zhou, Mingtao Li, Liejin Guo*, State Key Laboratory of Multiphase Flow in Power Engineering, School of Energy and Power Engineering, Xi'an Jiaotong University, 28, Xianning Street, Xi'an, Shaanxi 710049, China

From the viewpoint of photocatalysis, it is the anatase form of TiO_2 that is most important. Ti ions in the lattice were substituted by Ni ions to form Ni-doped TiO_2 which has been applied successfully for degradation of hazardous organic compounds or production of hydrogen or oxygen gas [1-4]. Therefore, a DFT calculation for the band structures and optical absorption spectra with varying Ni concentration in anatase TiO_2 models was conducted, in order to explore the effects of Ni doping on the band structure, photocatalytic property, and optical absorption spectrum.

The plane-wave pseudopotential method, implemented by CASTEP package [5], has been used to optimize crystal geometries, obtain the corresponding band structures and simulate the optical absorption spectra.

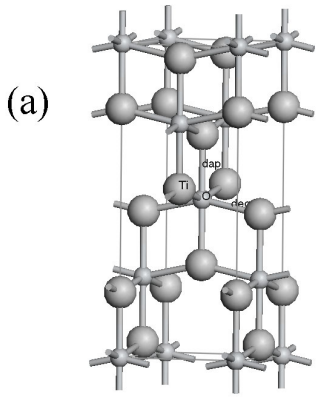

Figure 1: The crystal structure of pure TiO_2 (Model a).

2×1×1, 2×2×1, and 2×2×2 supercells with one Ti atom replaced by one Ni atom were denoted as Model (b), (c), and (d) to simulate doping concentration of 0.125, 0.062, and 0.031, respectively. Pure TiO_2 denoted as Model (a) was also calculated for comparison, as shown in Figure 1.

The optimized structural parameters of *a, c* and *u* ($u = d_{ap}/c$, d_{ap} is the apical Ti-O bond length) for pure anatase TiO_2 were listed in Table 1, which showed good consistence with

* Corresponding author, email address: lj-guo@mail.xjtu.edu.cn.

experimental [6] and theoretical results [7]. Six Ti-O bonds were contained in the distorted TiO_6 octahedron: d_{ap}=2.001Å and d_{eq}=1.941 Å, while d_{ap}=1.898Å and d_{eq}=1.919 Å in NiO_6 octahedron for Model (c) and (d). The local symmetry D_{2d} for the NiO_6 octahedron was remained in Ni doped TiO_2 with low Ni concentration. Mulliken population analysis [8] showed that the charge on the Ni ion was about 0.88, independent of its concentrations in the crystal and smaller than the charge (1.33) on the original Ti ion in this site. The adjacent six oxygen ions at vertices of the NiO_6 octahedron were slightly reduced. The charges on them were -0.61 in Model (c) and (d), while the charges on oxygen ions of the TiO_6 octahedron were -0.66.

Table 1: Structural parameters of anatase TiO_2.

	This work	Experimental [6]	FPLAPW [7]
a (Å)	3.785	3.782	3.692
c (Å)	9.718	9.502	9.471
u	0.206	0.208	0.206

Band structure plots for pure (Model a) and doped (Model c) TiO_2 were shown in Figure 2. It was indicated from Figure 2a that pure TiO_2 was an indirect band gap semiconductor with a minimum band gap of 2.13eV. The top of valence bands was near M point and the bottom of conduction bands was at G point. The underestimated band gap (3.2eV for experimental value) was well known for DFT method. After Ni doping, two dopant bands which were marked with solid squares (Figure 2c) appeared in the band gap of TiO_2. These bands were unoccupied, so they would be acceptor levels upon visible light excitation.

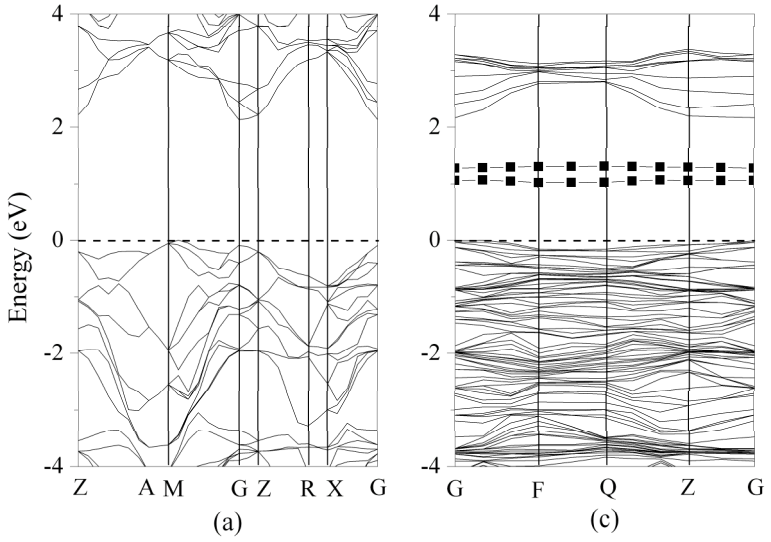

Figure 2: Band structure plots for pure (Model a) and doped (Model c) anatase TiO_2. The top of the valence band was denoted as zero.

Partial density of states (PDOS) plots calculated for TiO_2 with different concentrations of Ni impurity were presented in Figure 3. For pure TiO_2 in Figure 3(a), the upper valence bands showed a strong hybridization between O 2p and Ti 3d orbitals. The top of the valence bands was dominated by the O 2p orbitals, while the conduction bands, especially the bottom, contained significant contributions from the Ti 3d orbitals. It was obvious from Model (b), (c) and (d) in Figure 3 that the doped Ni 3d orbitals substantially contributed to the valence bands and the impurity bands. Two narrow bands (band I and II as shown in Figure 3c) were located in the middle of the band gap for Model (c) and (d). As Wang et al. [9] clarified for V doped TiO_2, the D_{2d} symmetry caused the three-fold degenerate t_{2g} ($3d_{xy}$, $3d_{xz}$, and $3d_{yz}$) and two-fold degenerate e_g ($3d_{x^2-y^2}$ and $3d_{z^2}$) of a transition metal cation to further split; the t_{2g} split into a two-fold degenerate level of both $3d_{yz}$ and $3d_{xz}$ and a level of $3d_{xy}$ while the e_g split into two levels of $3d_{x^2-y^2}$ and $3d_{z^2}$. Through a further examination of the orbital wavefunction contour maps of band I and II, the orbital contours for band I and band II showed the σ anti-bondings between O p_x or p_y orbital and Ni $d_{x^2-y^2}$ orbital and between O p_z orbital and Ni d_{z^2} orbital.

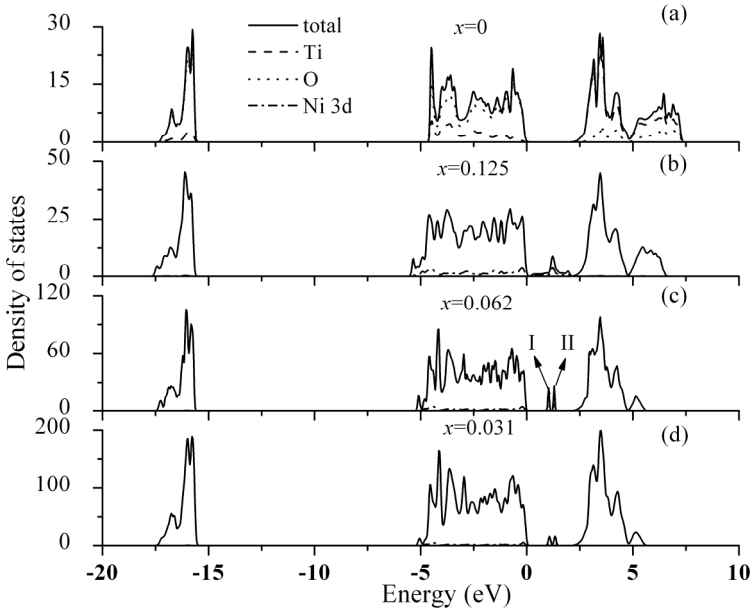

Figure 3: Partial density of states plots for different concentrations of Ni impurity in anatase TiO_2. The unit for density of states is electrons/eV, *x*: doping concentration.

In addition, Optical absorption spectra were calculated for different concentrations of Ni-doped anatase TiO_2 and the results were shown in Figure 5. The curve (a) for pure TiO_2 was calculated as a benchmark for comparing the results for Ni-doped TiO_2. For lower Ni impurity concentrations, curve (c) and (d) were very similar in the overall shape. The absorption for visible light with the characters of the shoulders around 450 nm and the tails reaching 700 nm was observed.

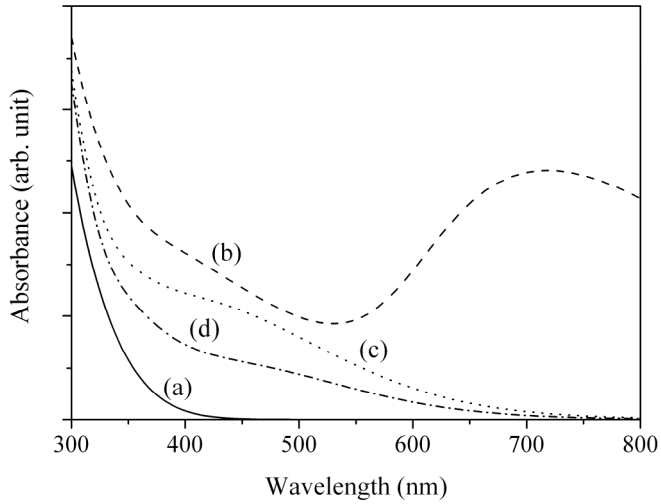

Figure 4: The optical absorption spectra for different concentrations of Ni impurity in anatase TiO_2 of the polycrystalline powder.

In summary, Ni doping had significant effect on electronic structure, optical absorption, and even photocatalytic property of anatase TiO_2. By introducing deep localized acceptor levels in the band gap, the response for visible light can be realized and the optical absorption spectra show the characters of the shoulder around 450 nm and the tail reaching 700 nm when Ni concentration approaches the experimental value. A schematic diagram of the band structure for Ni-doped anatase TiO_2 vs. normal hydrogen electrode (NHE) potential was drawn, as shown in Figure 5. This type of band structure was reasonable for the interpretation for various experimental phenomena.

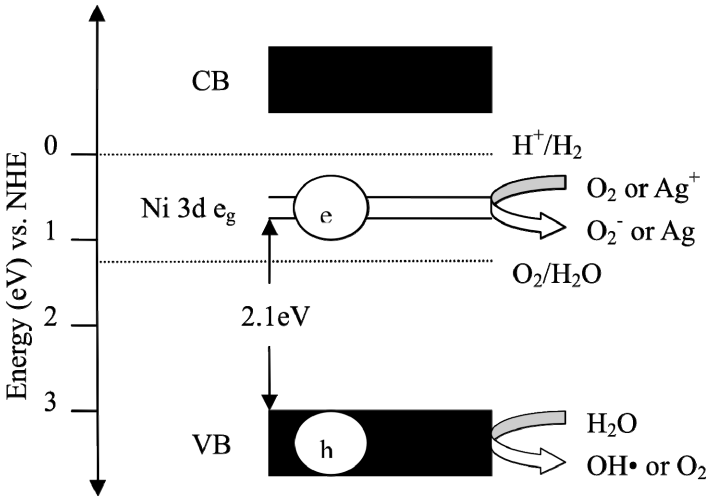

Figure 5: Schematic band structure diagram for Ni doped anatase TiO_2 vs. NHE potential.

Acknowledgments

The authors gratefully acknowledge the financial supports from the National Natural Science Foundation of China (Contracted No. 50821064), the National Basic Research Program of China (Contracted No. 2009CB220000) and the calculation resource supports from the molecular simulation computing platform in Xi'an Jiaotong University.

References

[1] S.D. Sharma, D. Singh, K.K. Saini, et al, Appl. Catal. A 314 (2006), 40-46.

[2] D.W. Jing, Y.J. Zhang, L.J. Guo, Chem. Phys. Lett. 415 (2005), 74-78.

[3] H. Yamashita, M. Harada, J. Misika, et al, Photoch. Photobio. A 148 (2002), 257-261.

[4] R. Niishiro, H. Kato, A. Kudo, Phys. Chem. Chem. Phys. 7 (2005), 2241-2245.

[5] M.D. Segall, P.L.D. Lindan, M.J. Probert, et al, J. Phys.: Condens. Matter 14 (2002), 2717-2744.

[6] J.K. Burdett, T. Hughbandks, G.J. Miller, et al, J. Am. Chem. Soc. 109 (1987), 3639-3646.

[7] R. Asahi, Y. Taga, W. Mannstadt, et al, Phys. Rev. B 61 (2000), 7459-7465.

[8] M.D. Segall, R. Shah, C.J. Pichard, et al, Phys. Rev. B 54 (1996), 16317-16320.

[9] Y. Wang, D.J. Doren, 136 (2005), 142-146.